ohio2/yjp-yjp/yjp-yjp/yjp99907/yjp9522d07z | xppws | 23:ver.3 | 5/13/10 | 15:58 | Msc: jp-2010-01836b | TEID: mlk00 | BATID: 00000

Confined Polar Mixtures within Cylindrical Nanocavities

Javier Rodriguez,[†,‡] M. D. Elola,[†] and Daniel Laria*[,†,§]

Departamento de Física, Comisión Nacional de Energía Atómica, Avenida Libertador 8250, (1429) Buenos Aires, Argentina, ECyT, UNSAM, Martín de Irigoyen 3100, (1650) San Martín, Provincia de Buenos Aires, Argentina, and Departamento de Química Inorgánica, Analítica y Química-Física e INQUIMAE, Facultad de Ciencias Exactas y Naturales, Universidad de Buenos Aires, Ciudad Universitaria, Pabellón II, (1428) Buenos Aires, Argentina

Received: March 01, 2010; Revised Manuscript Received: April 06, 2010

Using molecular dynamics experiments, we have extended our previous analysis of equimolar mixtures of water and acetonitrile confined between silica walls [*J. Phys. Chem. B* **2009**, *113*, 12744] to examine similar solutions trapped within carbon nanotubes and cylindrical silica pores. Two different carbon tube sizes were investigated, (8,8) tubes, with radius $R_{cnt} = 0.55$ nm, and (16,16) ones, with $R_{cnt} = 1.1$ nm. In the narrowest tubes, we found that the cylindrical cavity is filled exclusively by acetonitrile; as the radius of the tube reaches ∼1 nm, water begins to get incorporated within the inner cavities. In (16,16) tubes, the analysis of global and local concentration fluctuations shows a net increment of the global acetonitrile concentration; in addition, the aprotic solvent is also the prevailing species at the vicinity of the tube walls. Mixtures confined within silica nanopores of radius ∼1.5 nm were also investigated. Three pores, differing in the effective wall/solvent interactions, were analyzed, (i) a first class, in which dispersive forces prevail (hydrophobic cavities), (ii) a second type, where oxygen sites at the pore walls are transformed into polar silanol groups (hydrophilic cavities), and (iii) finally, an intermediate scenario, in which 60% of the OH groups are replaced by mobile trimethylsilyl groups. Within the different pores, we found clear distinctions between the solvent layers that lie in close contact with the silica substrate and those with more central locations. Dynamical modes of the confined liquid phases were investigated in terms of diffusive and rotational time correlation functions. Compared to bulk results, the characteristic time scales describing different solvent motions exhibit significant increments. In carbon nanotubes, the most prominent modifications operate in the narrower tubes, where translations and rotations become severely hindered. In silica nanopores, the manifestations of the overall retardations are more dramatic for solvent species lying at the vicinity of trimethylsilyl groups.

I. Introduction

The behavior of liquids under confinement continues to draw considerable attention. The interest responds to the dramatic changes that operate on the equilibrium and dynamical characteristics of these phases as the length scales that describe the spatial constraints become comparable to typical molecular sizes.[1] Besides the particular geometrical restrictions prevailing in such environments, another important variable that controls the behavior of confined liquids is the nature of the effective interactions at the domain boundaries. Near these interfaces, it is usual to observe important modifications in the intermolecular spatial correlations in the liquids. These modifications, in turn, may induce long-wavelength, collective responses leading, for example, to the stabilization of new phases which are absent in more conventional, bulk environments.[2−4] On the other hand, from the dynamical side, the overall effects of the confinement are normally translated into dramatic stretchings of all relevant time scales describing not only translational motion[5−7] but rotational[8−10] motions as well. As such, these modifications are key elements for the correct interpretation of many processes with practical applications, such as size-controlled fluxes,[11−16] gas storage,[17] and selective drug delivery.[18] In a much broader biological perspective, confining effects on aqueous phases is a relevant issue to understand the behavior of solvation shells that modulate the function of complex molecules and self-assembled structures, such as proteins,[19,20] DNA strands,[21] reverse micelles,[22] and lipid bilayers,[23] to cite a few important examples.

The examination of confined mixtures reveals equally interesting features. Most notable are those associated with preferential solvation phenomena and with modifications in the bulk-phase diagrams.[24−30] The latter modifications have been observed in nonpolar media[31−33] and polar solutions as well. Within the latter category, water−acetonitrile (W−ACN) mixtures provide a clear example. In a recent article, Kittaka et al.[34] have reported modifications in the melting and freezing temperatures of the solutions induced by solvation in MCM-41 mesopores.

We have recently reported molecular dynamics results describing the behavior of W−ACN equimolar mixtures confined between silica plates, held at fixed distances, intermediate between 0.85 and 1.5 nm.[35] Despite the narrow interval of interplate distances examined, we found a rich variety of solvation structures, also controlled by the characteristics of the plate/liquid interactions prevailing within the confining region. In a related context, we also undertook nonequilibrium molecular dynamics experiments to analyze the dynamics of local concentration fluctuations as two macroscopic phases composed by W and ACN are brought together through a membrane of carbon nanotubes.[36] The present paper combines common

* To whom correspondence should be addressed. E-mail: dhlaria@cnea.gov.ar.
† Comisión Nacional de Energía Atómica.
‡ UNSAM.
§ Universidad de Buenos Aires.

10.1021/jp101836b

ohio2/yjp-yjp/yjp-yjp/yjp99907/yjp9522d07z | xppws | 23:ver.3 | 5/13/10 | 15:58 | Msc: jp-2010-01836b | TEID: mlk00 | BATID: 00000

elements from these two previous studies. On the one hand, we will examine the behavior of W−ACN mixtures confined within smooth CNTs, with two different diameters, both close to 1 nm. On the other hand, we will also investigate the confining of similar mixtures within silica nanopores (SNP), with 3 nm diameters. In the latter case, three different pores will be considered, (i) a hydrophobic environment, where solid−liquid interactions only have dispersive contributions, (ii) a second, hydrophilic-like pore, where a sizable number of oxygen atoms at the solid interface are hydroxylated, and (iii) a third environment, where the topological disorder at the wall/liquid interface is augmented by transforming 60% of the previous OH groups into dangling, bulkier trimethylsilyl (TMS) groups. As such, the first part of our analysis will be focused on effects arising from the extent of the geometrical confinement on the liquid mixture, maintaining the wall/liquid interactions with no modifications. Conversely, in the second part, we will examine effects from wall functionalization.

The organization of the present paper is as follows. In the next section, we will describe the model and the technical details of our simulation experiments. Section III includes equilibrium results, whereas in section IV, we will present dynamical information for the mixtures. In section V, we will summarize the results along with some important concluding remarks.

II. Model

Confinement within CNTs was examined in fully periodic systems comprising a single tube immersed in equimolar liquid mixtures of W and ACN. The mixtures were first equilibrated at ambient conditions in a rectangular box of linear dimensions $L_x = L_y = 40$ Å and $L_z = 80$ Å. We then inserted an empty CNT at the center of the box, with its axis parallel to the z-direction, after removing the necessary solvent particles to avoid overlap between the tube and different solvent sites. This initial geometry was maintained throughout all runs by applying small harmonic restoring forces along the x- and y-directions ($k_{xy} \approx 15$ kcal mol^{-1} Å^{-2}) on four C atoms located at each rim of the tube. It is well-documented that this kind of constraint promotes minimal distortions in the dynamics of similar system.[37−39]

Two types of armchair CNTs were investigated, both with lengths close to $l_{cnt} \approx 60$ Å, an (8,8) tube, with radius $R_{cnt} \approx$ 5.5 Å, and a (16,16) tube, with $R_{cnt} \approx 11$ Å (see Figure 1a). The final numbers of solvent molecules were set to $N_W = N_{ACN} = 1000$ for the (8,8) tube. In simulations involving the (16,16) tube, the box was widened to $L_x = L_y = 60$ Å, and the total numbers of solvent molecules were taken up to $N_W = N_{ACN} = 2263$.

To model confinement within SNPs, we also considered fully periodic systems of linear dimensions $L_x = L_y = 51$ Å and $L_z \approx 80$ Å, containing $N_W = N_{ACN} = 1080$. The central portion of the simulation box was occupied by a solid silica slab, exhibiting a cylindrical pore of radius $R_s \approx 15$ Å, across the slab and along the z-axis, (see Figure 1b for additional geometrical details).

The silica pore was generated following closely the procedure described in previous papers.[40−44] Briefly, we started by considering a sample of fused SiO_2, confined within a rectangular box with $L_x = L_y = 51$ Å and $L_z = 31$ Å, at a density of 2.2 g cm^{-3}. The sample was equilibrated at $T \approx 8000$ K for about 250 ps, until all relevant thermodynamic variables attained equilibrium. We then partitioned the system into two regions, (i) a central, immobile, cylindrical resist along the z-axis, with radius $R_s \approx 15$ Å, surrounded by (ii) the rest of the liquid phase, in which the atoms were allowed to move. After further

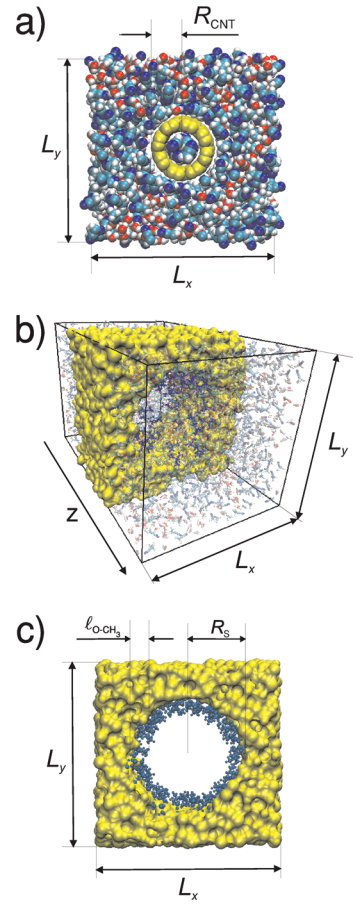

Figure 1. (a) Snapshot of a typical configuration of an (8,8) CNT filled exclusively with ACN. (b) Silica slab with a cylindrical pore immersed in a W−ACN mixture. (c) Silica pore functionalized with hydroxyl and trimethylsilyl groups (RHOC).

equilibration for about 100 ps, we brought the temperature down to ambient conditions by successive rescaling of the atomic velocities at a rate of $\Delta T \approx -100$ K every 4 ps. After reaching 298 K, the resist was removed, and we verified that the remaining external portion presented dynamical characteristics similar to those of an amorphous solid. The final stage of the procedure involved bringing together the resulting solid structure with the previously equilibrated sample of the liquid W−ACN mixture. From then on, the atoms comprising the solid silica remained immobile, whereas the liquid mixture was allowed to re-equilibrate and to permeate through the pore for about 500 ps. During this last stage, the length of the resulting simulation box along the z-axis was adjusted so as to bring the local composition and density of the mixture at the "bulk region", that is, $|z| \approx L_z/2$, in agreement with the experimental values observed in the corresponding macroscopic phases[45−47] (see Figure 1b).

Three different pores, differing in their interface structures, were examined. (i) The first ones, hereafter referred to as hydrophobic cavities (HOC), were modeled by assuming that liquid−solid site−site interactions were exclusively of the Lennard-Jones type. (ii) Effects from chemical functionalization in the pore walls were examined in hydrophilic cavities (HIC), in which dangling oxygen atoms lying at the pore interface were hydroxylated. Silanol groups were generated by attaching mobile hydrogen atoms to unsaturated fixed oxygen atoms, with a geometrical arrangement similar to the one described in ref 48. The total surface density of Si−OH groups was set to 0.03 Å^{-2}, which is in reasonable agreement with reported values obtained

ohio2/yjp-yjp/yjp-yjp/yjp99907/yjp9522d07z | xppws | 23:ver.3 | 5/13/10 | 15:58 | Msc: jp-2010-01836b | TEID: mlk00 | BATID: 00000

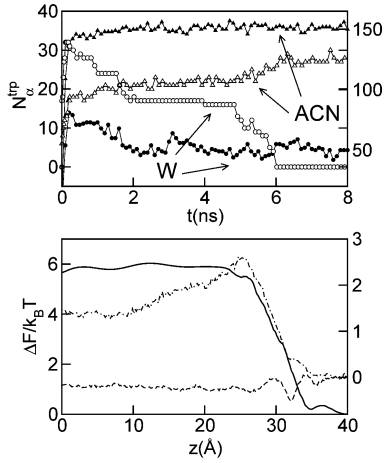

Figure 2. Top panel: Time evolution of the initial equilibration of confined molecules within carbon nanotubes of different radii. (8.8): open symbols, left axis; (16,16): black symbols, right axis. Bottom panel: Free energy for the confinement of W and ACN in CNTs. (8,8)/W: solid line, left axis; (16,16)/W: dash−dotted line, right axis; (16,16)/ACN: dashed line, right axis.

from gas adsorption experiments.[49] To obtain an adequate number of exposed oxygen sites available at the pore interface, we introduced embedded partial charges of magnitude ∼0.1 e in all of the sites comprising the central resist during the initial annealing process. (iii) Finally, we analyzed a more rugged hydrophobic cavity (RHOC) obtained by replacing ∼60% of the OH groups by bulkier mobile O−Si−$(CH_3)_3$ TMS ones. Note that, by incorporating the latter groups, the original extent of hydrophobicity at the pore wall was partially restored, whereas we also allowed for new sources of dynamical desorder. In addition, the resulting interface roughness was incremented due to new length scales associated with intramolecular distances within the TMS moieties which, in turn, modified effective solvent/wall interactions. The largest of these lengths roughly coincides with the distance between distal O−CH_3 groups, which is on the order of $l_{O-CH_3} \approx 4-5$ Å (see Figure 1c). Additional details pertaining to the adopted force fields and the simulation protocol are presented as Supporting Information.

III. Equilibrium Results

A. Confinement within Carbon Nanotubes. It will be instructive to start our analysis by examining the time evolution of N_α^{trp}, the populations of trapped species inside of the nanotubes, during a typical equilibration run. Results for both CNTs are shown in the top panel of Figure 2. One observes an initial interval lasting, say, ∼100 ps, during which the two species quickly fill the tubes. Note however that the populations after this short transient differ from the final concentrations in a sensible fashion. The most dramatic modifications occur for water in narrow tubes. After leveling off at an $N_W^{trp} \approx 19$ plateau-like value for $2 \lesssim t \lesssim 5$ ns, the corresponding curve sharply drops to zero after 6 ns. As such, our results indicate that hydrophobic cavities within CNTs with diameters up to ∼1 nm do not support trapped W and are exclusively filled with ACN. This phenomenon is akin to the one previously reported by us when we examined the behavior of polar mixtures confined between hydrophobic silica plates held at distances of ∼0.6 nm and presents similar characteristics to drying transitions in large hydrophobic cavities and CNTs dissolved in pure water.[48,50−53] For the larger (16,16) tubes, the modifications of the local concentrations are somewhat less spectacular, although still, compared to the bulk, there is a clear enhancement of the ACN concentration, in detriment to the water one, $N_{ACN}^{trp}/N_W^{trp} \approx 3$.

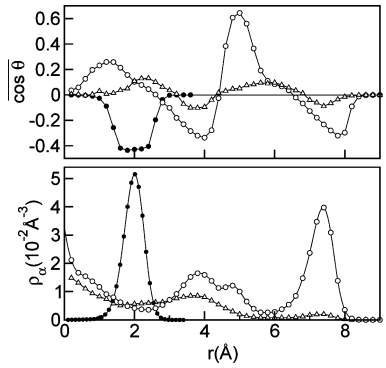

Figure 3. Polarization (top panel) and local density (bottom panel) fields for trapped mixtures inside of carbon nanotubes; ACN within (8,8) tubes (black circles), W within (16,16) tubes (open triangles), and ACN within (16,16) tubes (open circles).

The previous observations can be gauged from more quantitative grounds by considering free-energy profiles for the confinement process. In the bottom panel of Figure 2, we display results for, $F_\alpha(z)$, namely

$$F_\alpha(z) \propto -k_B T \ln\langle \delta(z_i^\alpha - z)\rangle_{R_{cnt}} \quad (1)$$

where $(x_i^\alpha, y_i^\alpha, z_i^\alpha)$ represents the coordinate of the ith particle of species α measured from a local system whose origin is at the center of mass of the tubular structure, k_B is the Boltzmann constant, and $\langle\cdots\rangle_{R_{cnt}}$ denotes an ensemble average restricted to a cylindrical section of the phase space of radius R_{cnt}. The profile for $\Delta F_W(z) = F_W(z) - F_W(\infty)$ for the (8,8) tube is dominated by a repulsive branch at the tube rims that prevents the spontaneous encapsulation of the solvent. Most likely, the microscopic origin of the barrier can be traced back to the rupture and reorganization of several hydrogen bonds. Note that the reversible work for the insertion of a W molecule is about ∼6 k_BT; therefore, in order to obtain a reasonable sampling for such infrequent fluctuations, we had to resort to an adaptive biasing force scheme.[54,55] This methodology has been successfully implemented in many analyses of encapsulation processes involving a large variety of guest−host partners.[38,39,56] In the wider (16,16) tube, the insertion of W molecules is still thermodynamically unfavorable, although the process involves going over a somewhat lower, that is, ∼2.3k_BT, barrier before reaching a plateau value of $\Delta F_W^\dagger = \Delta F_W(z=0) \approx 1.4 k_B T$ at the central section of the tubes. In contrast, the corresponding curve for ACN shows that this component is slightly more stable within the CNT than in the bulk, $\Delta F_{ACN}^\dagger \approx -0.16 k_B T$.

In addition to the modifications in the global concentrations, the geometrical characteristics of the confinement and the hydrophobic nature of the prevailing solvent−tube interactions also promote fluctuations in the local spatial correlations along length scales comparable to the radius of the tube. In Figure 3, we present results for radial density fields of the type

$$\rho_r^\alpha(r) = \frac{1}{4\pi r^2} \sum_i{}' \langle \delta(r_i^\alpha - r)\rangle \quad (2)$$

where the prime indicates a sum restricted to those molecules lying within the carbon nanotube and r_i^α corresponds to the distance between the ith molecule of species α and the axis of the tube (α is the central C site for ACN and the O site in W). The results for the smallest nanotube are depicted in the bottom

ohio2/yjp-yjp/yjp-yjp/yjp99907/yjp9522d07z | xppws | 23:ver.3 | 5/13/10 | 15:58 | Msc: jp-2010-01836b | TEID: mlk00 | BATID: 00000

panel, where only the ACN profile is shown. The curve looks like an off-centered Gaussian profile, located ~2 Å away from the cylinder axis. In (16,16) tubes, the results are dominated by a prominent peak at $r \approx 7$ Å, which corresponds to ACN in close contact with the wall of the tube, a region that appears practically devoid of water. On the other hand, effects of the confinement and the interactions of the wall gradually fade away in the central portion of the tube for distances of $r \lesssim 3$ Å, where both density profiles present values intermediate between 5×10^{-3} and 1.5×10^{-2} Å^{-3}. Note that the latter values are comparable to the experimental individual densities in equimolar bulk mixtures,[45−47] ~1×10^{-2} Å^{-3}.

Orientational correlations provide additional information about the structural characteristics of the confined liquids. In the top panel of Figure 3, we present results of

$$\overline{\cos\theta_\alpha}(r) = \frac{\sum_i{}'\langle\delta(\cos\theta_i^\alpha - \cos\theta)\delta(r_i^\alpha - r)\rangle}{\sum_i{}'\langle\delta(r_i^\alpha - r)\rangle} \qquad (3)$$

where θ_i^α represents the angle between the dipole moment of the ith molecule of species α and the radial direction in the cylinder. For the smallest nanotube, the average orientation of the ACN dipoles presents a non-negligible component along the radial direction $\overline{\cos\theta_{ACN}}$ (r≈2 Å) ≈ −0.45 and reveals that the negatively charged portions of the ACN molecules remain closer to the tube walls. The profiles for the dipolar alignment along the radial direction in wider tubes presents oscillatory behaviors for both species that still persist at small values of r. Also note that the less restrictive geometry allows for larger projections along the axial directions of the outer ACN dipoles, $\overline{\cos\theta_{ACN}}$ (r≈8 Å) ≈ −0.30, which benefit from stronger ACN−wall dispersive interactions.

B. Confinement within SiO_2 Nanopores. To analyze global concentration fluctuations within the different SNPs and in the flanking "bulk-like" spatial domains, we found it convenient to first consider density fields along the z-axis of the type

$$\rho_z^\alpha(z) = \frac{1}{\pi R_s^2}\sum_i\langle\delta(z_i^\alpha - z)\rangle_{R_s} \qquad (4)$$

Results for the three types of nanotubes are displayed in Figure 4 with open symbols. For HOC (top panel), one can see that the trapped liquid phase exhibits a clear enhancement of the ACN molecules ($N_{ACN}^{trp}/N_W^{trp} \approx 2$); conversely, in the lateral, bulk-like, regions (say, for $|z| \gtrsim 15$ Å), the mixture is richer in water ($N_{ACN}^{ltr}/N_W^{ltr} \approx 0.75$). The results that appear in the central panel reveal that, upon hydroxylation, the W and ACN overall concentrations in the pore become more comparable, the former being even slightly larger than the latter. Still, the nonuniform distribution of surface OH groups along the z-direction promotes irregular profiles for both ρ_z^α in the middle panel, most notably for $\rho_W(z)$ near the negative z rim of the pore. Finally, the replacement of two-thirds of the silanol by TMS groups brings both concentration profiles much closer to the originals for HOC (see bottom panel of Figure 4).

For HIC cavities, the asymmetries in the W and ACN profiles at the right- and left-hand sides persist even at bulk regions as one compares the individual curves at $z \approx \pm 15$ Å. As such, we do not discard that our results in these regions may be affected by additional confining effects arising from the periodicity of the simulation cell along the z-axis. In fact, the lateral reservoirs represent a single liquid phase "confined" between a pair of hydrophobic silica walls separated at a distance on the order of 45−50 Å. In order to investigate deeper into the extent of these effects, we also analyzed local density fluctuations sampled over the complementary region of phase space, that is, outside of the cylindrical section of radius R_s. The results are shown in Figure 4 with solid (ACN) and dashed (W) lines. The profiles are dominated by prominent maxima for ACN in contact with the lateral hydrophobic walls and, eventually, surrounding the pore gates. On the other hand, the structure of the water profiles is much less marked and converges toward the corresponding bulk densities after a couple of local maxima at $z = \pm 20$ and ±22 Å.

Plots of $\rho_r^\alpha(r)$ for the confined species in the pore are depicted in Figure 5. Given the already-mentioned irregularity in the distribution of OH and TMS groups along the z-axis, the results should be interpreted as density fields along the radial direction averaged over a collection of ~90 different functional groups

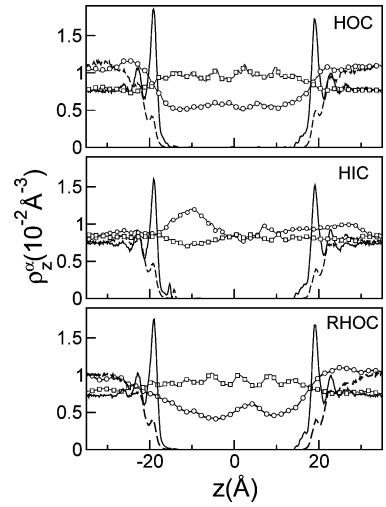

Figure 4. Local density fields along the z-axis of the simulation box for different silica pores. Samplings within a cylinder of radius R_s are shown in circles (W) and squares (ACN); samplings outside of that cylinder are shown with dashed (W) and solid (ACN) lines.

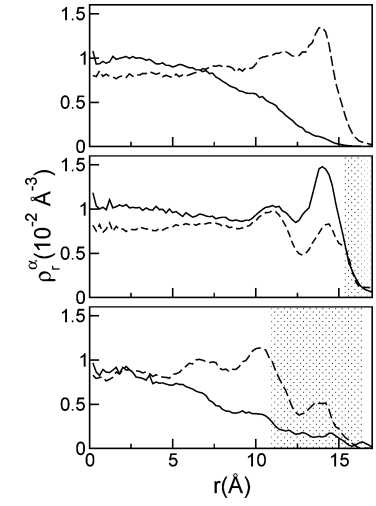

Figure 5. Local density fields along the radial direction for trapped W (solid line) and ACN (dashed lines) within different silica pores; HOC (top panel), HIC (middle panel), and RHOC (bottom panel). The shaded areas in the bottom and middle panel indicate the localization of OH and CH_3 groups in silanol and trimethylsilyl moieties, respectively.

TABLE 1: Dynamical Parameters for Confined Water−Acetonitrile Mixtures

(a) Carbon Nanotubes

type/species	τ_r^α (ns)	A_1	τ_1^α (ps)	A_2	τ_2^α (ps)	A_∞	$\langle\tau^\alpha\rangle^a$ (ps)
(8,8)/ACN	>5	0.55	48.6	0.16	2.13	0.29	
(16,16)/ACN	0.088	0.81	58.3	0.19	3.57	0.00	47.9
bulk mixture/ACN		1.00	5.9	0.00		0.00	5.9

(b) Silica Nanopores

type/species	τ_r^α (ns)	A_1	τ_1^α (ps)	β	$\langle\tau_1^\alpha\rangle^b$ (ps)	τ_2^α (ns)	$\langle\tau^\alpha\rangle^a$ (ns)
HOC/ACN	0.3	0.78	16.6	0.65	22.5	0.19	0.06
HIC/W	1.1	0.79	19.4	0.41	61.1	1.13	0.28
RHOC/ACN	1.4	0.52	33.64	0.39	116.4	2.49	1.25
bulk mixture/W		1.00	7.7	0.00	0.00	0.00	0.008

[a] Computed from the time integral of $C_\mu^{ACN}(t)$. [b] Computed from $\langle\tau_1^\alpha\rangle = \int_0^\infty e^{-(t/\tau_1^\alpha)^\beta}\, dt$.

located at the pore walls. Compared to the results for (8,8) and (16,16) nanotubes (bottom panel of Figure 3), fluctuations of the local densities within the roomier SNPs are somewhat less marked. Still, from qualitative grounds, HOC walls are preferentially solvated by ACN (see the broad peak along the $10 \lesssim r \lesssim 15$ Å interval in the top panel). Hydroxylation, in turn, promotes a larger extent of structure at the vicinity of the pore wall and reverses the previous preferential solvation as W now becomes the species that prevails near the walls. The analysis of the wall/solvent correlations at the vicinity of the silanol groups (not shown) reveals that OH groups, on average, receive one hydrogen bond from neighboring W molecules and also act as hydrogen-bond donors, with HO···O_W bonds being twice as frequent as HO···N_{ACN} ones. Near pore walls decorated with TMS groups, the previous structures appear very much blurred due to the wide variety of length scales involving wall/solvent interactions. Still, ACN seems to prevail across a much wider, $r \gtrsim 5$ Å, outer portion of the tube, while the water profile attains a bulk-like value only within the complementary central section of the pore.

IV. Dynamical Characteristics of Confined Mixtures

A. Carbon Nanotubes. The inhomogeneous characteristics of the spatial distributions of the confined mixtures also have consequences on their dynamics. For the sake of concision, in what follows, we will concentrate on dynamical features of molecules in close contact with the tube walls, where confinement effects should be more marked. This includes ACN particles near hydrophobic-like walls and W near hydroxylated ones. Following previous studies,[19,57,58] these domains were defined by inner radii set to $R_{cnt} = 6$ Å for the (16,16) CNT and $R_c = 10$ Å for the three types of SNPs. For (8,8) tubes, all molecules were included in the dynamical analysis. A more complete analysis including the rest of the species and internal layers within the nanotubes is postponed to a forthcoming publication.

Rough estimates of the residence times of the solvents in the outer domains were obtained from survival probabilities for molecules in contact with the tube walls of the type

$$N_\alpha(t) = \frac{\langle \eta_i^\alpha(t)\cdot\eta_i^\alpha(0)\rangle}{\langle(\eta_i^\alpha)^2\rangle} \qquad (5)$$

where $\eta_i^\alpha(t)$ equals 1 if the ith site of species α resides continuously adjacent to the wall for all times within the interval [0, t] and 0 otherwise. Characteristic residence times, τ_r^α, expressed in terms of time integrals of $N_\alpha(t)$ appear in the second column of Table 1. The magnitude of τ_r^α will be taken here as reference values for the longest time scales involving the temporal correlations that will be analyzed in the following paragraphs.

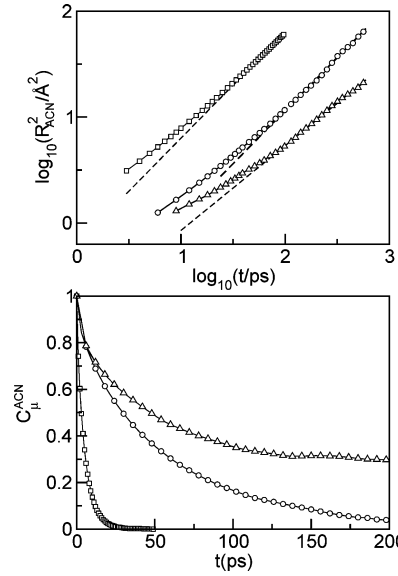

Figure 6. Top panel: Parallel mean-square displacements for ACN molecules trapped in CNTs of different diameter, in contact with the tube walls; (8,8) tube (triangles) and (16,16) tube (circles). The dashed lines, represent asymptotic behaviors $R_\alpha^2 \propto t^\alpha$, with $\alpha = 0.8$ for (8,8) tubes and $\alpha = 1$ for (16,16) tubes. Also shown are results for ACN in equimolar bulk mixtures, $\alpha = 1$ (squares). Bottom panel: Dipole−dipole relaxation for trapped ACN molecules in CNTs. Same labeling as that in the top panel.

Translational diffusion was analyzed by computing the parallel mean-square displacement defined as

$$\mathscr{R}_\alpha^2(t) = \langle |z_i^\alpha(t) - z_i^\alpha(0)|^2\rangle \qquad (6)$$

where the index i indicates particles that continuously remain within the outer tube domain, along the time interval [0, t]. Results for $\mathscr{R}_{ACN}^2(t)$ for CNTs are displayed in the top panel of Figure 6, where, as a reference, we have also included results from ACN in bulk mixtures. It is evident that translational modes of the ACN molecules in close contact with the tube walls exhibit a drastic slowdown, which becomes more dramatic as the tubes get narrower. As a quick reference to evaluate the extent of the retardation, note that, after 100 ps, the average

ohio2/yjp-yjp/yjp-yjp/yjp99907/yjp9522d07z | xppws | 23:ver.3 | 5/13/10 | 15:58 | Msc: jp-2010-01836b | TEID: mlk00 | BATID: 00000

displacement of an ACN particle within an (8,8) tube hardly exceeds its overall molecular size, whereas during a similar time period, the corresponding displacement along each coordinate in the bulk would be ~20 times longer (see the upper curve in the top panel of Figure 6). Similar observations have also been reported for pure ACN filling (8,8) CNTs, where, compared to the bulk value, the diffusion of the trapped molecules was shown to drop by a factor of ~4.5.[59]

In passing, we will briefly comment on the mechanisms that drive the diffusive modes within the tubes. The direct inspection of the curves shown in Figure 6 reveals that the long time dependence, say, $t \gtrsim 50$ ps, of $\mathscr{R}^2_{\mathrm{ACN}}(t)$ in the bulk and in (16,16) tubes looks reasonably linear. In contrast, the curve for (8,8) seems to be better described by power law, subdiffusive behavior of the type $\mathscr{R}^2_{\mathrm{ACN}}(t) \approx t^{\beta}$, with $\beta \approx 0.8$. Several studies, not always in agreement, have been undertaken in the past to examine the long time dependence of $\mathscr{R}^2(t)$ for fluids and gases confined within narrow CNTs. For example, a recent letter by Striolo[60] reports a dual behavior for trapped water in infinite long (8,8) CNTs, (i) a ballistic, that is, $\beta = 2$, regime at intermediate times followed by (ii) even faster motions beyond $t \gtrsim 500$ ps. On the other hand, Mukherjee et al.[61] have analyzed water motions in open-ended (6,6) CNTs and found Fickian diffusion at short times, followed by a drastic reduction in the time slope beyond ~200 ps. Finally, Alexiadis et al.[62] have recently reported a wide variety of β exponents, which seem to be dependent on the tube diameter and on details in the model Hamiltonian. At this point, we will only confirm that trajectories of ACN molecules trapped within (8,8) tubes exhibit characteristics similar to highly correlated single file diffusion, with no evidence of episodes during which a pair of molecules translocate positions. On the other hand, for (16,16) tubes, we did find events in which one particle surpasses a neighboring one without leaving the outer shell. A detailed analysis of these features and their consequences on the resulting behavior of $\mathscr{R}^2(t)$ is surely called for, although it is well beyond the scope of this paper; therfore, we will not proceed any further in our analysis.

Rotational dynamics of ACN molecules lying adjacent to the tube walls was examined by considering individual dipole−dipole time correlation functions of the type

$$C^{\alpha}_{\mu}(t) = \frac{\langle \boldsymbol{\mu}^{\alpha}_i(t)\cdot\boldsymbol{\mu}^{\alpha}_i(0)\rangle}{\langle |\boldsymbol{\mu}|^2\rangle} \qquad (7)$$

Plots for C^{ACN}_{μ} are displayed in the bottom panel of Figure 6, whereas characteristic time scales for rotational motions appear in columns 4, 6, and 8 of Table 1a. The latter values were obtained by assuming biexponential fits of the type

$$C^{\alpha}_{\mu}(t) = A_1 e^{-t/\tau^{\alpha}_1} + A_2 e^{-t/\tau^{\alpha}_2} + A_{\infty} \qquad (8)$$

The direct inspection of the plots in Figure 6 and the entries in Table 1a reveal important increments of the characteristic rotational time scales for the confined species. As a reference, the characteristic rotational time scale for ACN in (16,16) tubes, expressed in terms of $\langle\tau^{\mathrm{ACN}}\rangle$, the time integral of $C^{\mathrm{ACN}}_{\mu}(t)$, is already 1 order of magnitude larger than the one found in the bulk (see last column of Table 1a). As the diameter of the tube and the overall molecular size become comparable, rotations are even more severely hindered. Note that, in (8,8) tubes, the correlation function seems to attain a plateau-like value of $A_{\infty} \approx 0.3$ as t surpasses ~100 ps. The value of A_{∞} gauges the extent of orientational constraints acting on the trapped molecules. Assuming a random distribution of orientations, it is straightforward to relate the value of A_{∞} with θ_0, the largest amplitude of angular displacement;[63−67] for (8,8), such a calculation yields $\theta_0 \approx 50°$.

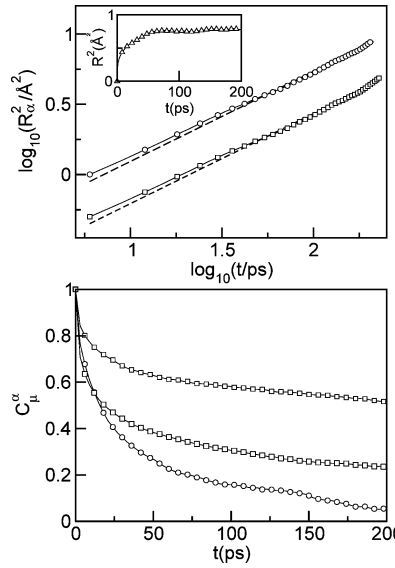

Figure 7. Top panel: Mean-square displacements for trapped species in silica pores lying close to the pore walls; HOC/ACN, circles; HIC/W, squares; RHOC/ACN, triangles. The dashed lines represent asymptotic behaviors $R^2 \propto t^{0.63}$. Bottom panel: Dipole−dipole relaxation for the same species as the top panel.

Coming back to the characteristics of $C^{\alpha}_{\mu}(t)$, for both nanotubes, the relaxations are dominated by main contributions from a $\tau_1 \approx 50-60$ ps branch, preceded by much faster relaxation processes characterized by $\tau_2 \approx 2-4$ ps. Interestingly, despite the larger degree of spatial restrictions prevailing in the smaller tubes, the characteristic time scales for (8,8) turn out to be somewhat smaller than those observed for the wider (16,16) tubes. This puzzling result is akin to the one reported by Kalugin et al.[59] for CNTs immersed in pure ACN and can be rationalized in terms of differences in the packing of ACN within tubes.

B. Silica Nanopores. The last part of our dynamical analysis will be focused on the behavior of mixtures within the SNPs and will follow a similar approach to the one that we performed in the previous section. The disparities between the entries for $\tau^{\alpha}_{\mathrm{r}}$ listed in Table 1b, almost a factor 5 for HOC and RHOC environments, already anticipate important effects from the functionalization on the dynamics of the closest solvation shell. Plots for the mean-square displacements appear in the top panel of Figure 7. The long time portions of the curves for HOC and HIC exhibit similar time dependence of the type $\mathscr{R}^2_{\alpha}(t) \propto t^{0.63}$. From a quantitative perspective, the net displacements next to the walls in HOC are comparable, albeit somewhat smaller, to those registered next to the CNT ones. Although there are clear differences in the magnitude of the wall/solvent dispersive interactions prevailing within CNTs and HOCs, one could speculate that the smoother nature of the CNT walls might facilitate the transport next to the tube walls. Hydroxylation brings into play strong hydrogen bond interactions with the adsorbed W molecules, and consequently, the parallel displacements become more hindered. Finally, the results for ACN near RHOC walls appear in the inset of the figure and suggest a completely different scenario. Note that after ~50 ps, the plot of $\mathscr{R}^2_{\mathrm{ACN}}(t)$ seems to level off at practically plateau values on

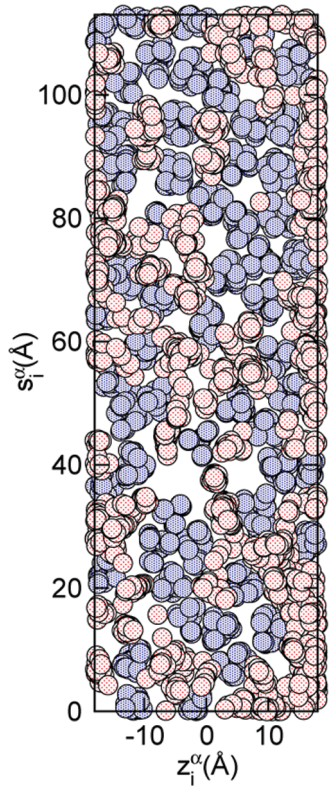

Figure 8. Projected coordinates of TMS groups (blue dark circles) and outer ACN groups (red light circles) onto a cylindrical surface of radius $R_{pr} = 18$ Å (see text) along a 1 ns trajectory. The diameter of each circle is 3 Å, which is a typical length scale to characterize site−site excluded volume interactions.

the order of ∼1 Å. As such, this would indicate the persistence of ACN molecules trapped within local potential minima, deep enough to prevent frequent jumps between adjacent wells. The picture that emerges from these considerations is accordant with an ACN−wall potential energy landscape of complex topology, which can be portrayed in terms of multiple wells modulated by the positions of the dangling TMS groups. As such, the translational dynamics near the wall would be dominated by small-amplitude, intrawell displacements, whereas transitions between adjacent wells seem to be described by temporal scales comparable to the average residence time at the outer shell. We remark that this description bears similar characteristics to those already described by Zang et al. for the transport of hydrogen-bonded liquids in aluminosilicate nanotubes.[68]

In order to bring additional support to this line of reasoning, in Figure 8, we present results for projected coordinates of the mobile atoms in TMS groups and the middle C atoms in ACN molecules, collected along a 1 ns trajectory. For the latter sites, only those located at the outer local maximum of ρ_r^C located at $r > 12.5$ Å were considered (see bottom panel of Figure 5). The projection was performed along local radial directions onto a cylindrical surface of radius $R_{pr} = 18$ Å. As such, the vertical axis refers to s_i^α coordinates defined in the following terms

$$s_i^\alpha = R_{pr}\theta_i^\alpha \qquad \cos\theta_i^\alpha = \frac{x_i^\alpha}{[(x_i^\alpha)^2 + (y_i^\alpha)^2]^{1/2}} \tag{9}$$

After 1 ns, the distribution of species clearly exhibits an irregular patchy structure in which the ACN remains mostly localized in manifold wells characterized by the absence of TMS groups, spread across the complete pore wall.[68]

Rotational relaxation plots appear in the bottom panel of Figure 7, whereas the characteristic time scales are listed in columns 4, 6, 7, and 8 of Table 1b. In these cases, the entries correspond to fits that combine simple and stretched exponentials of the type

$$C_\mu^\alpha(t) = A_1 e^{-(t/\tau_1^q)^\beta} + (1 - A_1)e^{-t/\tau_2^q} \tag{10}$$

Several observations are worth comment. (i) In all cases, the characteristic time scales of both contributions differ in a sensible fashion, with τ_2^q normally 1 order of magnitude longer than $\langle\tau_1^\alpha\rangle$. (ii) Contributions from the stretched exponential term, expressed in terms of the value of the A_1 weight, represent practically 80% of the total relaxation in HOC and become progressively less important as the overall rotational time scales increase. (iii) The overall rotational time scale for (16,16) CNTs and HOCs are still comparable, which is in agreement to what we have previously reported for the diffusive behavior. (iv) Rotational motions of W at the hydroxylated interface are 1 order of magnitude slower than those in the bulk mixtures (see results in the last row). (iv) Still, the most dramatic effects are those observed at the walls of RHOC. Note that the combination of the confinement and a highly rugose interface promotes an increment in the value of $\langle\tau^{ACN}\rangle$ of practically 3 orders of magnitude.

V. Concluding Remarks

The results presented in this paper reveal new features associated with the behavior of W−ACN mixtures as they get trapped within carbon tubular structures and cylindrical silica pores with nanometric dimensions. The CNT analysis allowed us to single out effects from the extent of the confinement, whereas the study of the SNPs focused on how functionalization modulates the characteristics of the confined mixtures.

From an equilibrium perspective, the most important modifications of these mixtures operate in local concentration fluctuations. Confinement effects bring additional complexity into the microscopic structures of the mixtures which, even in the isotropic bulk phase, are considered to be inhomogeneous at the mesoscopic scale.[69−74] Changes in the local concentrations are characterized by a variety of length scales, covering from those comparable to the overall size of the confining structure down to distances similar to typical molecular sizes. Concerning the first type, our analysis of confinement within CNT cavities showed the propensity of ACN to prevail within these hydrophobic-like environments. This tendency is made self-evident in narrow tubes with diameters close to and below 1.5 nm since they are filled exclusively by ACN. Note that this feature can be rationalized in terms of the very well known tendency of W to stay away from large hydrophobic surfaces.[52,53] Moreover, the extent of hydrophobicity was estimated by computing the free-energy profile for the encapsulation; in doing so, we found that such a process in (8,8) CNTs would typically involve surmounting a free-energy barrier on the order of $6k_BT$.

On the other hand, concentration fluctuations characterized by shorter length scales were also observed in the vicinity of the different tube walls. Most notably are those associated with the preferential solvation of ACN near hydrophobic-like walls and W in the vicinity of hydroxylated silica cavities. These inhomogeneities stretch out across typical distances on the order of 5 Å away from the tube walls, although they may also prevail

over even longer distances (~10 Å) for the case of RHOC, where the presence of dangling TMS groups broadens the local disorder at the pore walls.

From the dynamical side, in all cases, we registered important retardations in the translational and rotational modes. The similarity between the molecular size and the radius of the tube turns the diffusion of ACN molecules trapped in (8,8) nanotubes extremely slow and with a marked single-molecule character. The kinetic restrictions are even more severe for rotational motions where the geometrical constraints prevent full decorrelation of the relaxations.

In SNPs, we found similar trends. Dynamical modes of ACN next to HOC walls were found to be characterized by the fastest time scales. Hydroxylation, in turn, promoted considerable slowdowns in W motions. Finally, the presence of dangling TMS groups transformed the translational modes of the adsorbed ACN molecules into small-amplitude motions within potential wells, whose topology was dictated by the distribution of TMS groups at the surface. Under these circumstances, jumps between adjacent wells would be characterized by time scales similar to the overall residence time within the external solvation shell. In a similar fashion, interactions with the dangling groups would also bring the characteristic rotational time scales up to the nanosecond time domain.

Several important observations related to the results presented in this paper await proper rationalization. Most notably are those involving the origins of the anomalous dynamical behavior of the individual species, which was clearly reflected by the power law behavior of the mean-square displacements in narrow CNTs and the stretched exponential contributions at intermediate times of orientational relaxations in SNTs. Considering the reported behavior of water in contact with biological macromolecules, these anomalies are the result of a complex interplay which involved not only the dynamics of the substrate but also the geometrical and energetical characteristics of the underlying disorder.[19] Equally important will be the estimate of how far from the walls and beyond which threshold cavity size one recovers the usual bulk-like dynamical behavior. The answer to the latter issue will require a careful consideration of effective liquid/wall interactions and, once more, the characteristics of the disorder prevailing at the particular interface as well.

Another important issue to be addressed concerns the importance of the tightly adsorbed layer of ACN at the SNT's rims as controlling agents for in-and-out mechanisms of the trapping process, which should also modulate the diffusive characteristics of the external layers in close contact with the pore walls. In a recent paper, we have shown that this layer controls the ultraslow time behavior of the equilibration of fluxes across CNT membranes.[36]

Finally, and from a perspective focused on the structures of the binary mixtures, it would be important to explore systems in which hydrogen bonding controls the intermolecular connectivity of the two components on a more equal footing, such as water/methanol, for example. In a couple of recent papers, Zang et al.[68] and Jiang and collaborators[75] have described interesting behaviors of such mixtures within more regular carbon and metal oxide nanotubes, such as individual diffussive characteristics which differ at a qualitative level with the partial concentrations of the two components. Investigations along these lines are currently underway in our laboratory to assess the range of applicability of the picture presented here in these different scenarios.

Acknowledgment. J.R., M.D.E., and D.L. are staff members of CONICET (Argentina).

Supporting Information Available: Additional technical details concerning the simulation procedure. This material is available free of charge via the Internet at http://pubs.acs.org.

References and Notes

(1) Giovambattista, N.; Debenedetti, P. G.; Rossky, P. J. *Proc. Natl. Acad. Sci. U.S.A.* **2009**, *106*, 15181.
(2) Mashl, R. J.; Joseph, S.; Aluru, N. R.; Jakobsson, E. *Nano Lett.* **2003**, *3*, 589.
(3) Byl, O.; Liu, J.-C.; Wang, Y.; Yim, W.-L.; Johnson, J. K.; Yates, J. T., Jr. *J. Am. Chem. Soc.* **2006**, *128*, 12090.
(4) Jiang, J.; Sandler, S. I.; Smit, B. *Nano Lett.* **2004**, *4*, 241.
(5) Koone, N.; Shao, Y.; Zerda, T. W. *J. Phys. Chem.* **1995**, *99*, 16976.
(6) Yamaguchi, A.; Yoda, T.; Suzuki, S.; Morita, K.; Teramae, N. *Anal. Sci.* **2006**, *22*, 1501.
(7) Takahashi, R.; Sato, S.; Sodesawa, T.; Ikeda, T. *Phys. Chem. Chem. Phys.* **2003**, *5*, 2476.
(8) Farrer, R. A.; Fourkas, J. T. *Acc. Chem. Res.* **2003**, *36*, 605.
(9) Liu, G. Y.; Li, Y. Z.; Jonas, J. *J. Chem. Phys.* **1989**, *90*, 5881.
(10) Warnock, J.; Awschalom, D. D.; Shafer, M. W. *Phys. Rev. B* **1986**, *34*, 475.
(11) Jirage, K. B.; Hulteen, J. C.; Martin, C. R. *Science* **1997**, *278*, 655.
(12) Kalra, A.; Garde, S.; Hummer, G. *Proc. Natl. Acad. Sci. U.S.A.* **2003**, *100*, 10175.
(13) Martí, J.; Gordillo, M. C. *J. Chem. Phys.* **2001**, *114*, 10486.
(14) Martí, J.; Gordillo, M. C. *J. Chem. Phys.* **2003**, *119*, 12540.
(15) , G., H.; Rasaiah, J. C.; Noworyta, J. P. *Nature* **2001**, *414*, 188.
(16) Waghe, A.; Rasaiah, J. C.; Hummer, G. *J. Chem. Phys.* **2002**, *117*, 10789.
(17) Liu, C.; Fan, Y. Y.; Liu, M.; Cong, H. T.; Cheng, H. M.; Dresselhaus, M. S. *Science* **1999**, *286*, 1127.
(18) Singh, R.; Pantarotto, D.; Lacerda, L.; Pastorin, G.; Klumpp, C.; Prato, M.; Bianco, A.; Kostarelos, K. *Proc. Natl. Acad. Sci. U.S.A.* **2006**, *103*, 3357.
(19) Pizzitutti, F.; Marchi, M.; Sterpone, F.; Rossky, P. J. *J. Phys. Chem. B* **2007**, *111*, 7584.
(20) Pal, S. K.; Peon, J.; Zewail, A. H. *Proc. Natl. Acad. Sci. U.S.A.* **2002**, *99*, 1763.
(21) Pal, S. K.; Zhao, L. A.; Zewail, A. H. *Proc. Natl. Acad. Sci. U.S.A.* **2003**, *100*, 8113.
(22) Levinger, N. E.; Swafford, L. A. *Annu. Rev. Phys. Chem.* **2009**, *60*, 385.
(23) Lopez, C. F.; Nielsen, S. O.; L., K. M.; Moore, P. B. *J. Phys. Chem. B* **2004**, *108*, 6603.
(24) Gelb, L. D.; Gubbins, K. E.; Radhakrishnan, R.; Sliwinska-Bartkowiak, M. *Rep. Prog. Phys.* **1999**, *62*, 1573.
(25) Gelb, L. D.; Gubbins, K. E. *Phys. Rev. E* **1997**, *55*, R1290.
(26) Gelb, L. D.; Sliwinska-Bartkowiak, M.; Gubbins, K. E. *Fundamentals of Adsorption 6*; Meunier, F., Ed.; Elsevier: Paris, 1998.
(27) Rother, G.; Woywod, D.; Schoen, M.; Findenegg, G. H. *J. Chem. Phys.* **2004**, *120*, 11864.
(28) Woywod, D.; Schemmel, S.; Rother, G.; Findenegg, G. H.; Schoen, M. *J. Chem. Phys.* **2005**, *122*, 124510.
(29) Greberg, H.; Patey, G. N. *J. Chem. Phys.* **2001**, *114*, 7182.
(30) Hemming, C. J.; Patey, G. N. *J. Phys. Chem. B* **2006**, *110*, 3764.
(31) Formisano, F.; Teixeira, J. *J. Phys.: Condens. Matter* **2000**, *12*, A351.
(32) Formisano, F.; Teixeira, J. *Eur. Phys. J. E* **2000**, *1*, 1.
(33) Mao, Z.; Sinnott, S. B. *J. Phys. Chem. B* **2001**, *105*, 6916.
(34) Kittaka, S.; Kuranishi, M.; Ishimaru, S.; Umahara, O. *J. Chem. Phys.* **2007**, *126*, 091103.
(35) Rodriguez, J.; Elola, M. D.; Laria, D. *J. Phys. Chem. B* **2009**, *113*, 12744.
(36) Rodriguez, J.; Elola, M. D.; Laria, D. *J. Phys. Chem. B* **2009**, *113*, 14844.
(37) Hwang, H.; Schatz, G. C.; Ratner, M. A. *J. Phys. Chem. B* **2006**, *110*, 26448.
(38) Yu, Y. M.; Chipot, C.; Cai, W. S.; Shao, X. G. *J. Phys. Chem. B* **2006**, *110*, 6372.
(39) Yu, Y. M.; Cai, W. S.; Chipot, C.; Sun, T. T.; Shao, X. G. *J. Phys. Chem. B* **2008**, *112*, 5268.
(40) Gulmen, T. S.; Thompson, W. H. *Dynamics in small confining systems VIII*; Fourkas, J. T., Levitz, P., Overney, R., Urbakh, M., Eds.; Materials Research Society Symposium Proceedings, Warrendale, PA, 2006; Vol. 899E.
(41) Morales, C. M.; Thompson, W. H. *J. Phys. Chem. A* **2009**, *113*, 1922.
(42) Gulmen, T. S.; Thompson, W. H. *Langmuir* **2009**, *25*, 1103.
(43) Brodka, A.; Zerda, T. W. *J. Chem. Phys.* **1991**, *95*, 3710.
(44) Furukawa, S.; Nishiumi, T.; Aoyama, N.; Nitta, T.; Nakano, M. *J. Chem. Eng. Jpn.* **2005**, *38*, 999.

(45) Handa, Y. P.; Benson, G. C. *J. Solution Chem.* **1981**, *10*, 291.
(46) van Meurs, N.; Somsen, G. *J. Solution Chem.* **1993**, *22*, 427.
(47) Grande, M. D. C.; Alvarez-Juliá, J.; Marschoff, C. M.; Bianchi, H. L. *J. Chem. Thermodyn.* **2006**, *38*, 760.
(48) Giovambattista, N.; Rossky, P. J.; Debenedetti, P. G. *Phys. Rev. E* **2006**, *73*, 041604.
(49) Kamijo, T.; Yamaguchi, A.; Suzuki, S.; Teramae, N.; Itoh, T.; Ikeda, T. *J. Phys. Chem. A* **2008**, *112*, 11535.
(50) Giovambattista, N.; Debenedetti, P. G.; Rossky, P. J. *J. Phys. Chem. C* **2007**, *111*, 1323.
(51) Castrillon, S. R.-V.; Giovambattista, N.; Aksay, I. A.; Debenedetti, P. G. *J. Phys. Chem. B* **2009**, *113*, 1438.
(52) Chandler, D. *Nature* **2005**, *437*, 640.
(53) Chandler, D. *Nature* **2007**, *445*, 831.
(54) Darve, E.; Pohorille, A. *J. Chem. Phys.* **2001**, *115*, 9169.
(55) Hénin, J.; Chipot, C. *J. Chem. Phys.* **2004**, *121*, 2904.
(56) Rodriguez, J.; Semino, R.; Laria, D. *J. Phys. Chem. B* **2009**, *113*, 1241.
(57) Marchi, M.; Sterpone, F.; Ceccarelli, M. *J. Am. Chem. Soc.* **2002**, *124*, 6787.
(58) Faeder, J.; Ladanyi, B. M. *J. Phys. Chem. B* **2000**, *104*, 1033.
(59) Kalugin, O. N.; Chaban, V. V.; Loskutov, V. V.; Prezhdo, O. V. *Nano Lett.* **2008**, *8*, 2126.
(60) Striolo, A. *Nano Lett.* **2006**, *6*, 633.
(61) Mukherjee, B.; Maiti, P. K.; Dasgupta, C.; Sood, A. K. *J. Chem. Phys.* **2007**, *126*, 124704.
(62) Alexiadis, A.; Kassinos, S. *Mol. Simul.* **2008**, *34*, 671.
(63) Lipari, G.; Szabo, A. *Biophys. J.* **1980**, *30*, 489.
(64) Schröder, G.; Alexiev, U.; Grubmüller, H. *Biophys. J.* **2005**, *89*, 3757.
(65) Kinosita, K.; Kawato, S.; Ikegami, A. *Biophys. J.* **1981**, *20*, 289.
(66) Kawato, S.; Kinosita, K. *Biophys. J.* **1981**, *36*, 277.
(67) Rodriguez, J.; Mart, J.; Guardia, E.; Laria, D. *J. Phys. Chem. B* **2008**, *112*, 8990.
(68) Zang, J.; Konduri, S.; Nari, S.; Sholl, D. S. *ACS Nano* **2009**, *3*, 1548.
(69) Blandamer, M. J.; Blundell, N. J.; Burgess, J.; Cowles, H. J.; Horn, I. M. *J. Chem. Soc., Faraday Trans.* **1990**, *86*, 277.
(70) Marcus, Y.; Migron, Y. *J. Phys. Chem.* **1991**, *95*, 400.
(71) Kovacs, H.; Laaksonen, A. *J. Am. Chem. Soc.* **1991**, *113*, 5596.
(72) Bergman, D. L.; Laaksonen, A. *Phys. Rev. E* **1998**, *58*, 4706.
(73) Mountain, R. D. *J. Phys. Chem.* **1999**, *103*, 10744.
(74) Venables, D. S.; Schmuttenmaer, C. A. *J. Chem. Phys.* **2000**, *113*, 11222.
(75) Zheng, J; Lennon, E. M.; Tsao, H.-K.; Sheng, Y.-J.; Jiang, S. *J. Chem. Phys.* **2005**, *122*, 214702.

JP101836B